PAPER

Development and performance characterization of a compact plasma focus based portable fast neutron generator

View the article online for updates and enhancements.

Development and performance characterization of a compact plasma focus based portable fast neutron generator

Rishi VERMA[1,2] , Ekansh MISHRA[3] , Prosenjit DHANG[4],
Basanta Kumar DAS[1], Manraj MEENA[1], Lakshman RONGALI[1] and
Archana SHARMA[1,2]

[1] Pulsed Power & Electromagnetics Division, Bhabha Atomic Research Centre Facility, Atchutapuram, Vishakhapatnam 531011, India
[2] Homi Bhabha National Institute, Anushaktinagar, Mumbai 400094, India
[3] Raja Ramanna Centre for Advanced Technology, Rajendra Nagar, Indore 452013, India
[4] Variable Energy Cyclotron Centre, Bidhannagar, Kolkata 700064, India

E-mail: rishiv@barc.gov.in and rishiv9@gmail.com

Abstract

The design details and performance characterization results of a newly developed plasma focus based compact and portable system (0.5 m $\times$ 0.5 m $\times$ 1.2 m, weighing $\approx$100 kg) that produces an average neutron yield of $\sim$2 $\times$ 10^8 neutrons/shot (of fast D-D neutrons with typical energy $\sim$2.45 MeV) at $\sim$1.8 kJ energy discharge are reported. From the detailed analysis of the experimental characterization and simulation results of this system, it has been conclusively revealed that specifically in plasma focus devices with larger static inductance: (i) pinch current is a reliable and more valid neutron yield scaling parameter than peak current, (ii) the ratio of pinch/peak current improves as static inductance of the system reduces, (iii) the benign role of the higher static/pinch inductance ratio enables the supply of inductively stored energy in densely pinched plasma with a larger time constant and it is well depicted by the extended dip observed in the discharge current trace, (iv) there is the need to redefine existing index values of the pinch ($I_{\mathrm{pinch}}^{4.7}$) and peak ($I_{\mathrm{peak}}^{3.9}$) currents in neutron yield scaling equations to higher values.

Keywords: plasma focus, neutrons, time of flight, pinch current, peak current, plasma pinch, pseudospark switch

(Some figures may appear in colour only in the online journal)

1. Introduction

Dense plasma focus (DPF) is the simplest and least expensive source for producing a burst of neutrons in the short duration of a few tens of nanoseconds depending on the driver energy and other device parameters. For the purpose of neutron production, it is fueled either with pure deuterium (D_2) or a deuterium–tritium (DT) gas mixture [1]. The typical energy generated neutrons are $\sim$2.45 MeV with pure D_2 filling and $\sim$14.1 MeV with DT filling. This device was independently discovered by Mather [2] and Filippov [3] in the last century. A plasma focus (PF) tube mainly comprises a pair of coaxial electrode structures located inside the chamber that is filled with D_2/DT gas at low pressure. The anode at the centre is partially covered with a coaxial insulator near the back wall, and it is surrounded with squirrel-cage cathode rods in the outer periphery. By discharging capacitor bank energy through a fast closing switch, the plasma sheath is formed in between the electrodes and it is lifted upwards due to Lorentz force $\vec{J_r} \times \vec{B_\theta}$. After reaching the anode the top plasma sheath then starts imploding along the axis with a typical velocity of $\sim$$10^5$ m s^{-1} while compressing and heating a small volume of gas that reaches densities of $\approx$$10^{25}$ m^{-3} and temperatures of about $\approx$1 keV [4]. Coinciding with the disruption of this

hot and dense pinched plasma column due to rapid growth of magneto-hydrodynamic (MHD) instabilities, a burst of neutron is produced [5]. According to the beam-target hypothesis [6], a high voltage is generated due to fast disruption of the pinched plasma and this accelerates deuterons as a consequence of diode action. The interaction of these accelerated deuterons with hot dense plasma results in the production of neutrons.

Presently, owing to spin-offs from the Neutron Activation Analysis (NAA) application [7–10], there is a consistently growing demand for cost effective, compact and energy efficient, standalone and transportable types of neutron generators. In this context, our newly developed system satisfies the aforementioned requirements to a large extent. In the category of compact standalone pulsed power system (having single capacitor and switch) based DPF devices that have been developed across the globe [11, 12], this new system poses much lower inductance and it consequently results in a higher peak and pinch current, and therefore a relatively higher neutron yield [13] per Joule of stored energy. The overall size of this newly developed neutron source is just one-fourth of a previously developed source that produces an average neutron yield of $\sim 4 \times 10^9$ neutrons/shot at ~ 7 kJ discharge [14]. In this paper, along with a description of the system hardware design and construction, the results of characterization experiments carried out on this newly developed dense neutron generator with a closely integrated, compact, standalone pulsed power system are reported in detail. The five-phase Lee code (RADPFV5.13) [15] has also been used as a simulation tool to deduce and understand the corresponding changes in plasma dynamics and the pinch current parameter that is mainly responsible for a higher efficiency of neutron production in the newly developed PF device.

2. Experimental setup and diagnostics arrangement

The simple and energy-efficient pulsed power system of this small PF (SPF) device mainly comprises a single 12.5 μF/ 20 kV low inductance (<40 nH) metal-can energy storage capacitor and a maintenance-free sealed pseudospark switch along with its driver module. The pseudospark driver module provides a reservoir heater supply of ~ 5 V/2 A to control the hydrogen gas pressure inside the switch and ~ 5 kV fast impulse with a rise time <10 ns for its triggering [16].

To reduce the system inductance to minimum with enhanced reliability in operation, all the major parts of this neutron generation system (i.e. capacitor bank, switch and PF chamber) have been closely integrated without the use of flexible cables. A constructional schematic illustrating the assembly of the scheme is shown in figure 1. The anode of the pseudospark switch is rigidly connected over the capacitor head, whereas its discharge end to load (i.e. the cathode) directly interfaces with the anode of the PF chamber. The coaxial configuration of the current return helps in minimizing the overall system inductance and ensures symmetric flow of the discharge current, which further helps in balancing and
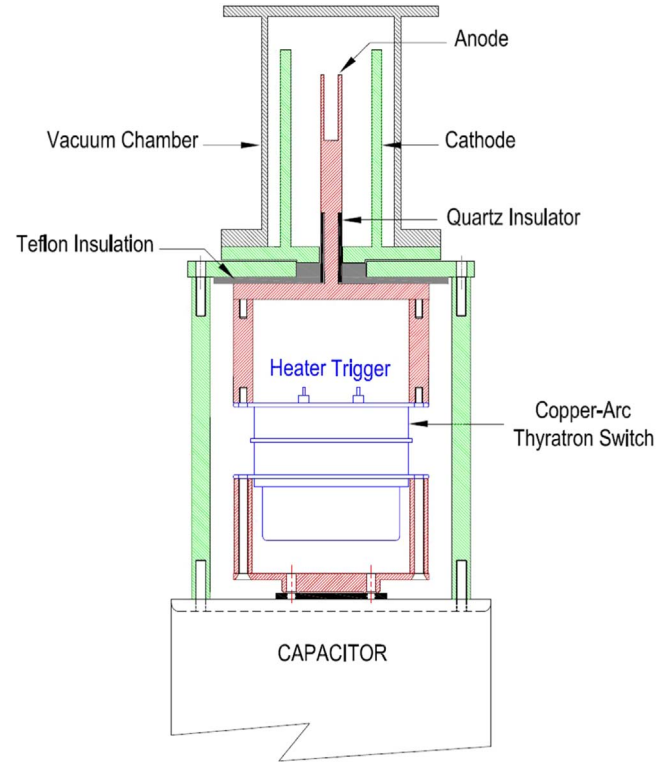

Figure 1. Construction and integration of various parts of the SPF device.

Table 1. Major specifications of the compact pulsed neutron source.

Item		Parameter
DD neutron yield per pulse	:	$\geqslant 2 \times 10^8$ (average)
Neutron energy (DD)	:	~ 2.45 MeV (typical)
Neutron pulse duration (FWHM)	:	~ 35 ns (typical)
PF head	:	Replenishable & demountable type
Minimum time interval between shots	:	1 min (minimum)
Total energy stored (E_o)	:	2.5 kJ (maximum)
Total capacitance (C_o)	:	12.5 μF
Charging voltage (V_{ch})	:	20 kV (maximum)
Energy transfer switch	:	Pseudospark
Peak discharge current (I_{peak})	:	200 kA (maximum)
Size of demountable PF head	:	0.1 m (ϕ) $\times$ 0.2 m (h)
Overall weight of the system	:	100 kg (approx.)
Overall size of the system	:	0.5 m $\times$ 0.5 m $\times$ 1 m

distributing mechanical stresses generated due to electromagnetic forces. The specifications of this compact neutron generator are highlighted in table 1.

The stainless steel anode of 100 mm length (z_o) and 8 mm radius (a) is concentrically placed through the squirrel-cage cathode structure in which six 8 mm diameter brass rods are fixed on a circular radius of 35 mm (b). To minimize the
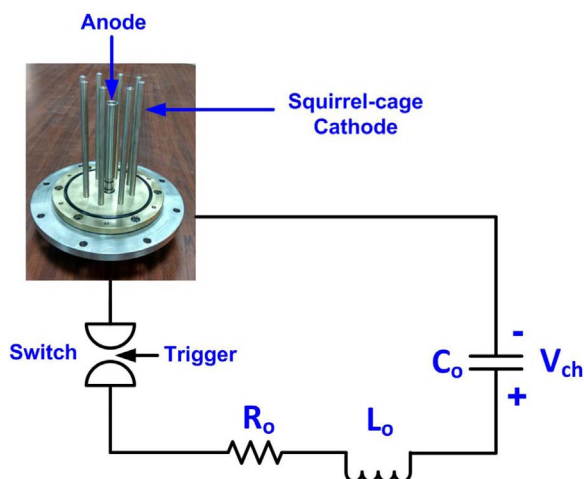
Figure 2. A schematic representing the main electrical parameters of the PF device.

detrimental effect of the addition of ablated impurities into hot dense plasma from the anode top, a cylindrical hole of 11 mm diameter and 50 mm depth is bored at the centre of the anode. A quartz glass tube of 25 mm length with an inner/outer diameter of 12 mm/16 mm has been used as an insulator sleeve. In between the anode and ground return plates, a 5 mm thick Teflon® sheet has been used as sandwiched insulation. The PF chamber enclosing the coaxial electrode assembly has major dimensions of 0.1 m (ϕ) × 0.2 m (h). As all the hardware parts are compactly integrated, residual inductance of ∼75 nH was obtained for the total system (contributed by the capacitor, switch and PF tube), and this enables delivery up to ∼200 kA peak current (at maximum rated voltage) in the quarter time period of about ∼1.5 μs. The circuit parameters of the PF device in conjunction with an actual snap of the coaxial electrode assembly are shown in figure 2. C_o is the total capacitance that is charged to a suitable voltage level V_{ch}, and L_o and R_o are the static inductance and resistance, respectively, of the total electrical circuit.

As seen in the system photograph shown in figure 3, all the auxiliaries like a high voltage charger, pseudospark switch driver and other protection circuitry are housed within the same system cabinet. A constant current power supply of 30 kV/10 mA rating (procured from M/s Ionics Power Solutions Ltd, India) has been used for the charging of the capacitor bank. A 100 kΩ series resistance is used while charging to protect the charging power supply from high reverse voltage (that is generated during discharge) [17]. Under adverse circumstances when the pseudospark switch fails to fire, then the entire energy stored in the capacitor is dumped through a solenoid operated switch into a 3 kΩ stack of series-connected bulk ceramic composition disc resistors. Optical–electrical and electrical to optical transmitter-receiver links of 50 m length are used for firing the neutron generator.
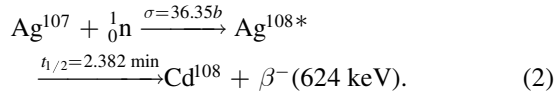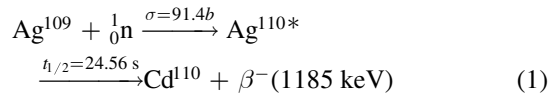
The diagnostics used for analyzing the performance of the SPF device are: (i) a Rogowski coil as an electrical diagnostic tool for probing the current derivative (di/dt) and seed current ($\int I(t)dt$) signals. These signals provide comprehensive information regarding axial acceleration and radial

**Figure 3.** The standalone compact pulsed neutron generator.

collapse/pinch phase plasma dynamics and, hence, are the most important indicators of the PF device performance; (ii) a silver activation counter (SAC) and ^{3}He detector for the neutron yield measurements. The SAC has been used for many years in several small and large DPF facilities for measuring the pulsed neutron yield due to its following inherent advantages: (1) neutron yield information is safely preserved in the counter after the exposure of neutron burst, (2) it has a sufficiently high cross section for thermal neutrons, (3) the short half life of its two stable isotopes enables rapid measurement with the use of simple counters, (4) a dynamic range of measurements with the SAC can cover a few orders of magnitude of neutron intensity depending on its dimensions [18]. It is remarkable to note that silver has two isotopes Ag^{107} and Ag^{109} with abundance of 48.17% and 51.83%, respectively. Neutrons emitted from the PF device are slowed down while passing through the moderator of

optimal thickness and induce two radiative capture nuclear reactions (see equations (1) and (2)) in the foil that is made of natural silver [18]:

$$Ag^{109} + {}_0^1n \xrightarrow{\sigma=91.4b} Ag^{110}*$$
$$\xrightarrow{t_{1/2}=24.56\,s} Cd^{110} + \beta^- (1185\ keV) \quad (1)$$

$$Ag^{107} + {}_0^1n \xrightarrow{\sigma=36.35b} Ag^{108}*$$
$$\xrightarrow{t_{1/2}=2.382\,min} Cd^{108} + \beta^- (624\ keV). \quad (2)$$

In the utilized setup, a silver foil thickness of $\sim$250 μm has been used as activation material and is wrapped around three thin-walled Geiger–Muller (GM) tubes (LND-719), and they are symmetrically placed at the centre inside a hydrogen-reach cylindrical moderator of high-density polyethylene (HDPE) of major dimensions with 150 mm diameter and 350 mm height. The diameter of each hole is 18 mm and the depth is 280 mm. All three GM tubes are biased at +900 V DC and their paralleled output is fed as input to the linear amplifier (LA); then, the LA output goes into the counter/timer unit that registers counts for a defined period. During the experiments, the silver activation detector setup was placed at a distance of 1 m from the source and it has a calibration factor of 2×10^5 neutrons/count. The beta particles that are the result of silver activation reach the GM counter and finally produce the electrical impulses, which are proportional to the number of neutrons falling on the detector in 4πsr

A high sensitivity ^{3}He proportional counter in 'charge integration mode' (CIM) has also been used for the secondary confirmation of the neutron yield in 4πsr [19]. The cross section for the ^{3}He reaction is $\sim$5330 barns for thermal neutrons, and the detection principle is based on the nuclear reaction shown below [20]:

$$^3He + n \rightarrow {}^3H + {}^1H + 765\ keV. \quad (3)$$
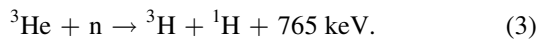
As may be noted from the given nuclear reaction, the neutron causes the break-up of the nucleus into tritium nucleus, ^{3}H and a proton, ^{1}H. The triton and proton share the 765 keV reaction energy. Thus, the amount of energy deposited by this nuclear reaction leads to the release of energetic charged particles into the gas and, consequently, the produced multiplicative ionization reveals the detection of neutrons. The ionization potential of helium is about 25 eV. About $\sim$25 000 ions and electrons are produced per neutron interaction (cumulating charge of $\sim 4 \times 10^{-15}$ Coulombs) [20]. A ^{3}He neutron detector tube (#25He3/456/25NS) of nominal sensitivity 50 cps/nν has been used, and it is centrally placed inside the cavity of size 30 mm (ϕ) $\times$ 350 mm (h) in a cylindrical moderator (i.e. hydrogenous plastic material Delrin^{TM}) with major dimensions of 200 mm (ϕ) $\times$ 500 mm (h) and $\sim$80 mm thick wall for thermalizing neutrons. A preamplifier with a typical gain of $\sim$150 mV pC^{-1} was used for conditioning of the signal obtained from the ^{3}He detector, and its output is fed directly to the oscilloscope. To register the time-resolved history of generated hard x-rays (HXR) and neutrons, a detector assembly of a plastic scintillator (NE-102A with a thickness and diameter of 50 mm) coupled with a

photomultiplier tube (EMI 9813BK) has been used. For electromagnetic shielding this detector assembly was enclosed inside a tightly capped light-proof aluminum housing [21]. When the high energy photons of several tens to hundreds of keV strike on the plastic scintillator, its molecules get excited, and while de-excitation occurs, visible radiation is emitted. On the other hand, when 2.45 MeV energy neutrons strike on the plastic scintillator, molecular excitation is produced by transferring energy to recoil protons [22]. When the emitted light that is followed by de-excitation falls on the photocathode of the attached photo-multiplier tube, photoelectrons are generated and multiplied producing a current pulse recorded in a fast oscilloscope. Experimental data were acquired on two digital storage oscilloscopes (Agilent DSO-7104B, 4 GS/s, 1 GHz) and a computer, and these were placed inside a Faraday cage to prevent the noise coupling.

3. Results and discussion

To standardize the performance of this compact neutron generator, the discharge voltage was kept fixed at $\sim$17 kV for all shots, and the D_2 filling gas pressure was incrementally varied from 2 to 8 mbar. Consecutively, five shots were taken at each setting to obtain the average neutron yield. For the absolute measurement of pressure, a rugged barometrically compensated 'capsule dial gauge' (#CG16K) from Edwards Vacuum^{TM} was used. It covers the measuring range of 0 to 25 mbar, and has an accuracy of $\pm$2% of full scale deflection.

It has been well established that the radiation yield of the PF device maximizes when the focusing/pinching occurs at the instant while the discharge current is at its peak [22]. Since the velocity of the current sheath in the axial and radial phases is predominantly governed by the D_2 gas pressure inside the chamber, hence it becomes important to investigate the optimum pressure at which maximum neutron yield is obtained for a particular discharge current or stored energy [22, 23]. The time evolution traces of typical current (*I*) and current derivative (d*i*/d*t*) signals (with a dip at the first quarter time period), which were monitored by the Rogowski coil at $\sim$17 kV/5 mbar discharge, are shown in figure 4.

It may be noted from figure 4 that the progression of the current sheath from the breakdown phase to the completion of the axial rundown phase takes $\sim$1.5 μs, and then the radial phase, including the final pinch breaking up, is typically over in <100 ns duration. Observation of multiple pinches as displayed in the time profile of the current and current derivative signals as a consequence of dynamic growth in plasma instabilities is quite random. However, some earlier studies on this aspect [24, 25] have revealed its increasing/decreasing occurrences with filling gas pressure. The efficient pinch compression is verified by a strong dip in the current derivative signal, which is due to the rapid change in plasma impedance attributed by (i) fast-changing plasma inductance $L_p(t)$, and (ii) growth in anomalous resistance $R_p(t)$ caused by the collision of electrons with plasma waves when they reach a high intensity level [26]. The higher magnitude of a distinct, sharp dip implies stronger pinching [27] resulting in efficient
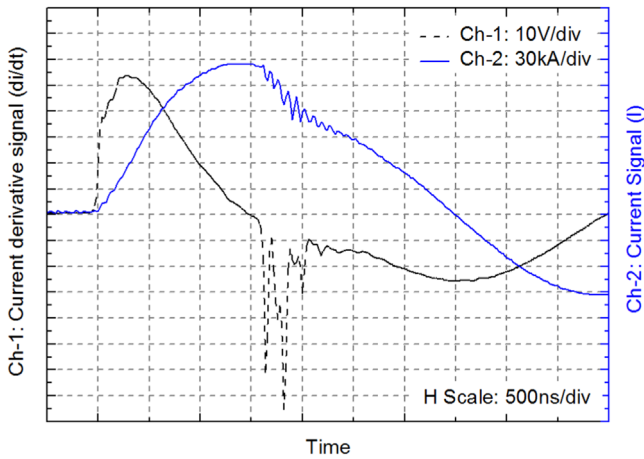
Figure 4. Oscilloscope traces of typical current and current derivative signals for discharge at ~17 kV/5 mbar.
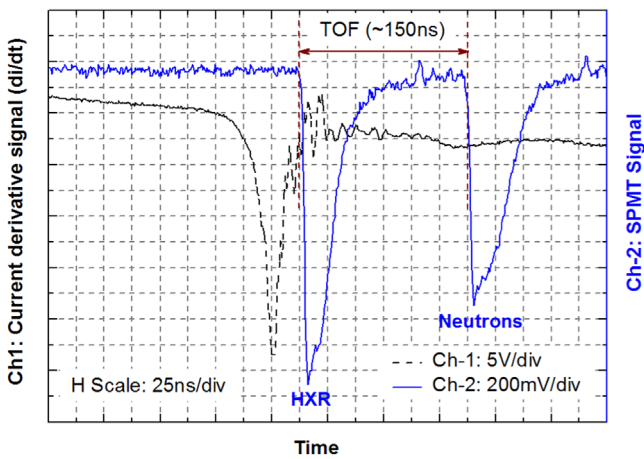

Figure 5. The signal from the SPMT detector placed at 3.2 m distance in the side-on direction.

Figure 6. The ^{3}He detector output signal through the charge sensitive preamplifier.

radiation emission from the pinched plasma column producing a burst of HXR and fusion neutrons. HXR and neutron pulses were discriminated on the basis of time-of-flight (TOF) signals obtained from the scintillator–photomultiplier (SPMT) detector assembly [28] that was placed at a distance of ~3.2 m from the source. Figure 5 shows the measured TOF signal for a shot at ~5 mbar D_2 filling gas pressure. The time difference of ~25 ns between the dip of the d*i/*d*t* signal and the first peak of the SPMT detector signal is due to dissimilar cable lengths.

The typical travelling speeds of x-rays and 2.45 MeV neutrons are ~3×10^{10} cm s^{-1} and ~1.96×10^9 cm s^{-1}, respectively; thus a time delay of ~150 ns between the two pulses obtained from the SPMT detector confirms their simultaneous generation from the PF device [22]. The measured average pulse durations of the HXR and neutron pulse were 30 ± 3 ns and 37 ± 6 ns, respectively.

The time-integrated neutron yield in each pulse was measured using the SAC and ^{3}He detector in the proportional counter mode, and they are placed at a distance of 1 m from the PF axis in the side-on direction. Neutron yield estimation
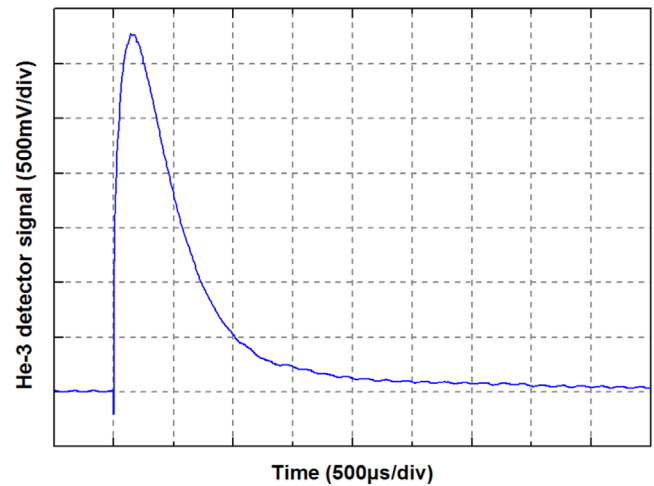
using the SAC was simply carried out by measuring the jump in counts (due to induced activity in silver foil by interaction with themalized neutrons) that is immediately followed after the discharge, and then the product of the net measured counts (after deducting the background) with a calibration factor gives the final measure of the neutron yield. The counting duration was set to 300 s to reduce the effect of statistical fluctuations between counting. Also, to obtain a more realistic estimate, prior to each discharge, a record of background counts was taken, and it was deducted from the total counts measured after the discharge. For the secondary confirmation of the measured neutron yield, a ^{3}He detector was also used. The ^{3}He detector tube signal obtained at a bias setting of +600 V is shown in figure 6. The area under this signal is then estimated and multiplied by the calibration factor (i.e. 240 neutrons/μVs) to estimate the neutron yield [19]. It is worth mentioning here that the estimated calibration factor is specific to the bias voltage setting and the calibrated distance between the source and detector.

The measured average neutron yield and time-to-pinch (i.e. time between the start of the breakdown phase until the end of the radial compression phase) at various D_2 pressures are shown in figure 7. The filling gas was periodically refreshed to reduce the effect of contamination on radiation yields.

As shown in figure 7, a maximum average neutron yield of ~$(2.3 \pm 0.3) \times 10^8$ neutrons/shot was produced at a D_2 gas pressure of ~5 mbar. The corresponding time-to-pinch was ~1.5 μs. The further increase observed in the time-to-pinch at increased pressures is due to excess loading on the current sheath [23]. It is clearly evidenced from the shown results that the PF device produces maximum neutron yield only in a particular pressure range [29].

This observation is also supported by the thermonuclear and beam-target hypothesis of neutron production [27]. It is remarkable to note that neutron yield in a wide energy range of PF devices conventionally follows the proportionality of peak current with an index of ~4 (i.e. I^4) [13]; subjected focusing/pinching occurs at the instant while the discharge
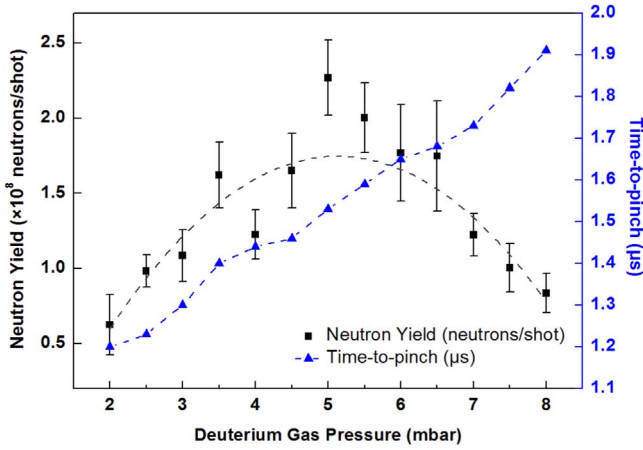
Figure 7. Average neutron yield and time-to-pinch versus D_2 gas pressure.

Figure 8. The measured and 'fitted' current trace for operation at 17 kV/5 mbar.

current is at its peak. Practical realization of this condition has interdependence on anode length, peak current/charging voltage and filling gas pressure. Since the anode length and peak current/charging voltage are fixed, then the D_2 gas pressure is the only variable parameter that was fine-tuned to satisfy the conditions for obtaining the optimum neutron yield.

A plausible explanation for relatively lower neutron yields at low pressures is higher acceleration of the current sheath that consequently results in much faster growth of Rayleigh–Taylor (RT) instability and breaking of the pinched plasma column prematurely [30]. At optimum pressure, the plasma sheath gets adequately slowed down thereby increasing the RT instability growth time that enhances compression of the pinched plasma column to higher density. A consequent increase in confinement duration and density thus results in a higher reaction rate probability and more neutron yield [31]. It is clearly evidenced in the shown results that increasing the pressure beyond the optimal range causes the time-to-pinch to increase further at a later instant when the discharge current has crossed its peak. Heating of pinched plasma reduces at less current and, therefore, the neutron yield reduces. It is also important to note that for efficient focusing with pure D_2 filling, the specific energy of the plasma sheath must be $\geqslant 1$ MJ/g for swept mass to produce the optimum neutron yield [23, 32].

The reported average neutron yield of some similar energy range PF devices [11, 12, 33] and that of our PF device are shown in table 2 for comparison purposes. The relative comparison of average neutron yield (Y_n) versus stored energy (E_o) clearly indicates that this new system poses a higher neutron yield than the other listed devices per Joule of stored energy.

It is remarkable to note that the neutron yield scales with peak (I_{peak}) and pinch (I_{pinch}) currents as $Y_n \sim (9 \times 10^9) \times I_{peak}^{3.9}$ and $Y_n \sim (2 \times 10^{11}) \times I_{pinch}^{4.7}$ [13], where the I_{peak} typically ranges from 0.1 MA to 3.2 MA and the I_{pinch} typically ranges from 0.1 MA to 1.2 MA. Experimentally, the peak value of the total current (I_{peak}) that is fed into the PF tube is the most commonly measured electrical parameter
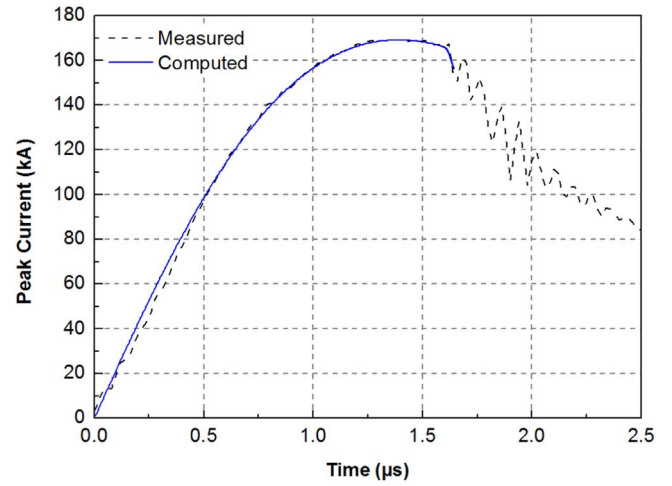
using a Rogowski coil. The pinch current (I_{pinch}) that actually participates in the focusing phase is very difficult to measure experimentally as the probe causes electromagnetic perturbation to pinch. It has been widely observed that neutron yield scales more consistently with I_{pinch} as it directly powers all the emission processes [13]. The beam target is the dominant mechanism of neutron production in a wide energy range of PF devices across the globe, and its relation is given as [6]:

$$Y_{b\text{-}t} \approx C_n n_i\, I_{pinch}^2\, z_p^2\, \ln(b/r_p)\, \sigma / V_{max}^{1/2} \qquad (4)$$

where I_{pinch} is the current flowing through the pinch at the start of the slow compression phase, n_i is the ambient ion density, r_p is the radius of the plasma pinch, b is the cathode radius, σ *is* the cross section for the fusion reaction, V_{max} is the maximum voltage induced by the current sheath collapsing radially towards the axis and C_n is a constant. Neutron yield estimation using this beam-target mechanism is comprehensively included in the five-phase Lee model RADPFV5.13 [15].

In the present work, actual values of I_{peak} and I_{pinch} from the measured total discharge current waveform are deduced by fitting a numerically computed current trace upon an experimentally measured current trace by suitably adjusting the swept mass factor f_m/f_{mr} and the current shedding factor f_c/f_{cr} for the axial/radial phases, respectively, in the Lee code [34]. Plasma dynamics in all three major phases of the PF device operation and its efficient focusing are clearly evident in the discharge current trace signal obtained on the oscilloscope [22].

The primary inputs required for running the Lee code [15, 34] are the capacitor bank parameters (C_o, L_o and R_o), the focus tube parameters (a, b and z_0) and the operational parameters (V_{ch}, p and filling gas properties). It is also important to note that since the code is charge-consistent, and L_o and R_o vary dynamically during focusing action, the computed amplitude of the peak current is a more accurate value than the measured amplitude. A 'fitted' discharge

Table 2. A relative comparison of E_o and Y_n reported by various laboratories.

DPF device	Energy E_o (kJ)	Average neutron yield Y_n (neutrons/shot)
SPF (this work)	1.8	$(1–2) \times 10^8$
KSU-DPF [12]	1.8	$(1–2) \times 10^7$
UNU-ICTP [11]	2.7	$(0.5–1) \times 10^8$
NX–2 [33]	2.9	$(6–8) \times 10^8$

Table 3. Model parameters and simulation results obtained for various DPF devices.

DPF devices	I_{peak} (kA)	I_{pinch} (kA)	C_o (μF)	L_o (nH)	R_o (mΩ)	f_m	f_c	f_{mr}	f_{cr}	Speed factor (kA/cm√Torr)	Estimated neutron yield (neutrons/shot)
SPF (this work)	170	142	12.5	75	8	0.06	0.68	0.28	0.8	109	$\sim 2 \times 10^7$
KSU-DPF [12]	137	94	12.5	123	14.4	0.10	0.70	0.20	0.7	105	$\sim 3.5 \times 10^6$
UNU/ICTP [11]	164	110	30	110	12	0.08	0.70	0.16	0.7	100	$\sim 1 \times 10^7$
NX-2 [33]	448	260	28	20	3.8	0.15	0.50	0.32	0.7	75	$\sim 8.5 \times 10^8$

current trace of the SPF device for operation at 17 kV/5 mbar D_2 gas pressure is shown in figure 8. The fine-tuned electrical 'circuit parameters' and values of the 'model parameters' that have been obtained for 'best fit', along with 'peak and pinch current' estimations for all the DPF devices listed in table 2 are summarized in table 3.

As the estimated peak/pinch currents are 170 kA/142 kA at ~ 17 kV discharge in the SPF, therefore, according to suggested empirical scaling equations [13] as well as from the Lee code, a neutron yield typically in the order of $\sim 10^7$ neutrons/shot is expected; however, experimentally, a one order higher magnitude of neutron yield, i.e. $\sim 2.3 \times 10^8$ neutrons/shot, was measured. This unexpected superior yield may be defended by the extended current dip with good depth and duration observed in the discharge current trace that is shown in figure 8. From the fitting of the computed current trace over the measured trace it may be seen that the experimentally measured dip in the discharge current trace signal extended much beyond the computed dip. All iterations were attempted using model parameters, but the computed current dip could not be made to fit over the extended portion of the measured current dip.

A comprehensive review of various parameters of DPF devices shown in tables 2 and 3 reveal that the SPF, KSU-DPF [12] and UNU-ICTP [11] devices fall into the category of systems with higher circuit inductance [35], and their experimentally measured and computed neutron yield typically differ by an order of magnitude, whereas in NX-2 like devices, those that have very low circuit inductance, good agreement is observed in such systems between measured and computed neutron yields [35]. A plausible explanation regarding the anomaly in measured and computed neutron yields and the noticeable signature of the long extended dip in the discharge current trace in PF devices of higher circuit inductance is mainly due to a higher ratio of static and pinch inductance, i.e. $(L_o + L_a)/L_p$, where L_o is the static residual circuit inductance of the PF device, L_a is the dynamic inductance of the axial part of the focus tube and L_p is the dynamic pinch inductance that is typically in the range of 5

nH to 10 nH. This higher inductance ratio results in bulk residual inductive energy that is gradually transferred into the pinch instabilities with a larger time constant. The signature of a strong extended dip in the discharge current trace is mainly the consequence of a rapid change in plasma impedance attributed by fast-changing plasma inductance $L_p(t)$, and rapid growth in anomalous resistivity $R_p(t)$. Hence, the 1/e time scale (i.e. L_p/R_p depicted as an extended dip in the current trace) in which the current drops to $\sim 37\%$ is mainly decided by the lumped circuit parameters [34, 35].

Further review of the Lee code simulation results shown in table 3 for various DPF devices also infers that circuit inductance L_o has a crucial role in limiting the peak/pinch currents that may be extracted from per kJ of stored energy. The SPF and KSU-DPF [12] were both operated at the same stored energy of ~ 1.8 kJ, but the I_{peak}/I_{pinch} currents were 172 kA/142 kA and 137 kA/94 kA, respectively. The higher I_{peak}/I_{pinch} in our SPF device is mainly the consequence of $\sim 40\%$ smaller circuit inductance (i.e. ~ 75 nH) than KSU-DPF (i.e. ~ 123 nH) [12]. Similarly, it may be noted that even though the SPF and UNU-ICTP [11] devices were operated at different stored energies of ~ 1.8 kJ and ~ 2.7 kJ but their extracted peak currents (I_{peak}) are nearly the same, i.e. 170 kA and 164 kA, respectively, because of 30% less circuit inductance in the SPF device (i.e. 75 nH versus 110 nH), conversely a higher fraction of current goes into the pinch of the SPF device and thus results in a relatively higher neutron yield (at least $\sim 2\times$) at $\sim 33\%$ less stored energy than the UNU-ICTP [11] device.

It is remarkable to note that the 'speed factor' is typically about 89 ± 8 kA cm^{-1} Torr$^{-1/2}$ in a wide energy range of D_2 fuelled PF devices, and it is basically the measure of driving magnetic energy per unit mass associated with the peak discharge current [36]. In all the PF devices with higher system inductance [35] as listed in table 3, the values of the speed factor for the neutron optimized regime are typically in the range of 100 to 110 kA cm^{-1} Torr$^{-1/2}$ indicating that the plasma sheath speed in these devices in the axial and radial phases is relatively on the higher side than their normal range,

attributing better compression and higher shock heating of the pinched plasma column [37] and thus supporting enhanced radiation yield.

4. Conclusion

The newly designed and developed SPF device has been successfully demonstrated as a compact, efficient pulsed neutron source producing an average yield of $\geqslant 2 \times 10^8$ neutrons/shot with pure D_2 filling that may be conveniently utilized for various applications, such as NAA, calibration and testing of newly developed fast/thermal neutron detectors, and testing the shielding/moderation effectiveness of fast neutrons in new composite materials. The closely packed hardware integration in a small unit has played a crucial role in limiting the static system inductance (L_o) $\leqslant 75$ nH. The design of the PF electrode dimensions is well matched with the electrical characteristics of the driving current pulse, allowing maximum pinch compression to coincide with the peak of the discharge current in a quarter time period of about ~ 1.5 μs. In conclusion, causes of the higher neutron generation efficacy of the newly developed SPF device in comparison to other devices with stored energies in a similar range are enumerated as follows.

1. A reduction in static inductance (L_o) of the electrical circuit enhances the peak current and pinch current, which in turn enhance the neutron yield.

2. From the experimental measurements and Lee code simulation results, it is clearly evident that the I_{peak} and I_{pinch} mainly depend on the value of the static inductance L_o compared to the dynamic inductances of the PF. As L_o is reduced, the ratio of I_{pinch}/I_{peak} improves and, e.g. irrespective of the different energy stored in the SPF and UNU-ICTP [11] devices, both systems deliver peak currents in the similar range as 170 kA and 164 kA, respectively; but the pinch current is higher in the SPF device than the UNU-ICTP [11] device (142 kA versus 94 kA) owing to less circuit inductance (75 nH versus 110 nH). This case study also concludes that the I_{peak} alone cannot be considered as a valid neutron yield scaling parameter, especially for the devices with significantly different and higher L_o. Better consistency in neutron yield scaling has been demonstrated with I_{pinch} as the reliable scaling parameter [38].

3. Observation of extended dip in discharge current traces with higher depth and duration depicts the influence of higher system inductance in conserving large inductive energy. The higher static/pinch inductance ratio $(L_o + L_a)/L_p$ helps in the gradual transfer of stored energy into the pinch until the end of the radial compression phase with a larger time constant [34, 35]. Hence, it is realized that L_o also has a pivotal role in enhancing the stabilization of the high-density pinched plasma column enriching the beam-target mechanism for neutron generation.

4. The presented results and analysis also infer that, for the more realistic estimation of neutron yields in PF devices with higher static/pinch inductance ratios [35], more data need to be collected and analyzed to obtain updated index values of I_{pinch} and I_{peak} in scaling equations [13] as scaling parameters.

5. The speed factor/drive parameter is an indicative measure of the speed of plasma in both the axial and radial phases, and its noticeable constancy in the higher range of 100 to 110 kA cm^{-1} Torr$^{-1/2}$ along with strong focusing characteristics corroborates higher shocked heating and better compression of the pinched plasma column resulting in enhanced neutron yield.

Acknowledgments

ORCID iDs

Rishi VERMA ⓘ https://orcid.org/0000-0002-0106-3279
Ekansh MISHRA ⓘ https://orcid.org/0000-0003-3731-9296

References

[1] Mikhailov Y V, Lemeshko B D and Prokuratov I A 2019 *Plasma Phys. Rep.* **45** 334
[2] Mather J W 1965 *Phys. Fluids* **8** 366
[3] Filipov N V, Filipova T I and Vinogradov V P 1962 *Nucl. Fusion* **2** 577
[4] Peacock N J *et al* 1972 *European Conf. on Controlled Fusion and Plasma Physics*
[5] Hirano K and Yamamoto T 1988 *Phys. Fluids* **31** 2710
[6] Lee S 2014 *J. Fusion Energy* **33** 319
[7] Tomar B S *et al* 2013 *Nucl. Instr. Meth. Phys. Res. Sect.* A **703** 11
[8] Andola S *et al* 2014 *Nucl. Instr. Meth. Phys. Res. Sect.* A **753** 138
[9] Milanese M *et al* 2013 *Rev. Sci. Instrum.* **84** 103501
[10] Gribkov V *et al* 2006 *AIP Conf. Proc.* **875** 415
[11] Lee S *et al* 1988 *Am. J. Phys.* **56** 62
[12] Abdou A E *et al* 2012 *IEEE Trans. Plasma Sci.* **40** 2741
[13] Lee S and Saw S H 2008 *J. Fusion Energy* **27** 292
[14] Verma R *et al* 2016 *Rev. Sci. Instrum.* **87** 095102
[15] Lee S and Saw S H 2010 *Energies* **3** 711
[16] Bochkov V D *et al* 1998 *Instrum. Exp. Tech.* **41** 676
[17] Bushnell A H 2002 Interfacing pulsed power systems to switching power supplies *Proc. 25th Int. Power Modulator Symp., 2002 and 2002 High-Voltage Workshop* (Piscataway, NJ: IEEE) 290
[18] Jednorog S *et al* 2014 *J. Radioanal. Nucl. Chem.* **301** 23
[19] Moreno J *et al* 2008 *Meas. Sci. Technol.* **19** 087002
[20] Ahmed S N 2015 *Physics and Engineering of Radiation Detection* (Amsterdam: Elsevier) (https://doi.org/10.1016/C2013-0-15270-1)
[21] Verma R *et al* 2012 *IEEE Trans. Plasma Sci.* **40** 3280

[22] Milanese M M *et al* 2007 *IEEE Trans. Plasma Sci.* **35** 808

[23] Milanese M, Moroso R and Pouzo J 1993 *IEEE Trans. Plasma Sci.* **21** 606

[24] Behbahani R A and Aghamir F M 2011 *Phys. Plasmas* **18** 103302

[25] Yousefi H R *et al* 2006 *Phys. Plasmas* **13** 114506

[26] Bernard A *et al* 1977 *Nucl. Instr. Methods* **145** 191

[27] Castillo F *et al* 2000 *J. Phys. D Appl. Phys.* **33** 141

[28] Bruzzone H *et al* 2010 *IEEE Trans. Plasma Sci.* **38** 1592

[29] Pouzo J O and Milanese M M 2003 *IEEE Trans. Plasma Sci.* **31** 1237

[30] Bilbao L and Bruzzone H 1984 *Phys. Lett.* A **101** 261

[31] Beg F N *et al* 2002 *Appl. Phys. Lett.* **80** 3009

[32] Alfvén H 1942 *Stockholm Observatoriums Annaler* **14** 114

[33] Koh J M *et al* 2005 *Plasma Sources Sci. Technol.* **14** 12

[34] Lee S *et al* 2008 *Appl. Phys. Lett.* **92** 111501

[35] Lee S *et al* 2011 *J. Fusion Energy* **30** 277

[36] Lee S and Serban A 1996 *IEEE Trans. Plasma Sci.* **24** 1101

[37] Acuña H, Bernal L and Pouzo J 1994 *Proc. 1994 Int. Conf. Plasma Physics* 125

[38] Lee S and Saw S H 2017 The plasma focus—numerical experiments, insights and applications ed R S Rawat *Plasma Science and Technology for Emerging Economies: An AAAPT Experience* (Singapore: Springer) p 113